Atmospheric Environment 219 (2019) 117005

Contents lists available at ScienceDirect

Atmospheric Environment

journal homepage: http://www.elsevier.com/locate/atmosenv

Hydration of acetic acid-dimethylamine complex and its atmospheric implications

Jie Li [a], Ya-Juan Feng [a], Shuai Jiang [a], Chun-Yu Wang [a,b], Ya-Juan Han [b], Cai-Xin Xu [a], Hui Wen [b], Teng Huang [b], Yi-Rong Liu [a,**], Wei Huang [a,b,c,*]

[a] School of Information Science and Technology, University of Science and Technology of China, Hefei, Anhui, 230026, China
[b] Laboratory of Atmospheric Physico-Chemistry, Anhui Institute of Optics & Fine Mechanics, Chinese Academy of Sciences, Hefei, Anhui, 230031, China
[c] CAS Center for Excellent in Urban Atmospheric Environment, Xiamen, Fujian, 361021, China

HIGHLIGHTS

- Clusters consisting of HOAc, DMA and H2O are relatively stable.
- Water molecules make the hydrogen bond in HOAc-DMA stronger.
- High RH could promote the HOAc-DMA cluster growth.
- Hydration could decrease the evaporation rates of HOAc and DMA.

ARTICLE INFO

Keywords:
Nucleation mechanism
Acetic acid
Topological analysis
Atmospheric relevance
Formation rate

ABSTRACT

Atmospheric aerosols are closely related to weather, climate and human health, and New particle formation (NPF) is a major source of atmospheric aerosols. Currently, some field observations and experiments indicate that acetic acid (HOAc) could be involved in NPF events. However, mechanism of acetic acid nucleation is still unclear. In this study, the low-lying structures and thermodynamics of acetic acid (HOAc)-dimethylamine (DMA)-water (W) system were studied at PW91PW91/6–311++G (3df, 3pd) level. We found that acetic acid forms relatively stable clusters with dimethylamine, and that proton transfer enhances the strength of the hydrogen bond in (HOAc) (DMA) $(H_2O)_n$ (n = 2–4) clusters. Temperature has an important effect on the distribution of isomers, especially for (HOAc) (DMA) $(H_2O)_2$ clusters. Besides, all the isomers contribute to the nucleation of clusters. The various RH has a negligible effect on the hydrate distribution. However, the non-hydrated clusters are always dominant and they are easy to form stable cluster, as seen from the comparison of hydrate distributions and cluster formation rates. The above analyses indicate that (HOAc) (DMA) is relatively stable and some larger clusters based on (HOAc) (DMA) may participate in new particle formation.

1. Introduction

Atmospheric aerosols have a tremendous impact on Earth's radiation budget, photochemistry, human health, and climate (Zhang et al., 2007; Saxon and Diaz-Sanchez, 2005; Saikia et al., 2016; Li et al., 2005; Makkonen et al., 2012; Baker and Peter, 2008; Kulmala et al., 2004). New particle formation (NPF) contributes to atmospheric aerosol formation and dominates concentrations of cloud condensation nuclei (CCN) (Kulmala, 2003; Merikanto et al., 2009). Although nucleation phenomena have been intensively investigated in the past, role of some nucleating species and nucleation mechanisms are yet not well understood (Lanz et al., 2007; Zhang et al., 2011; Bzdek et al., 2012), especially in the case, when small molecular clusters are nucleating (Chen et al., 2017a; Junninen et al., 2010; Jokinen et al., 2012; Zhao et al., 2010).

Sulfuric acid (SA) has been proved as a critical aerosol nucleation precursor through numerous field observations and laboratory studies (Vehkamäki et al., 2002; Sipilä et al., 2010; Kurtén et al., 2008). However, since the concentration of sulfuric acid in the range of 10^5 to 10^7 cm^{-3} is not large enough to explain the measured nucleation events

* Corresponding author. School of Information Science and Technology, University of Science and Technology of China, Hefei, Anhui, 230026, China.
** Corresponding author.
E-mail addresses: yrliu@ustc.edu.cn (Y.-R. Liu), huangwei6@ustc.edu.cn (W. Huang).

https://doi.org/10.1016/j.atmosenv.2019.117005
Received 29 March 2019; Received in revised form 20 September 2019; Accepted 24 September 2019
Available online 30 September 2019
1352-2310/© 2019 Elsevier Ltd. All rights reserved.

in the actual atmospheric environment, other species could be involved in the nucleation events (Kuang et al., 2010; Kulmala and Kerminen, 2008; Paasonen et al., 2010), such as ammonia, ionic species, and organic compounds (Kurten et al., 2006; Han et al., 2018; Nadykto and Yu, 2007; Nadykto et al., 2008a, 2008b, 2009, 2014, 2018; Herb et al., 2011, 2012; Ortega et al., 2008; Olenius et al., 2013; Bork et al., 2011a, 2011b; Zhang et al., 2004, 2009; Kildgaard et al., 2018; Lv et al., 2018; Kupiainen-Määttä et al., 2014; Ryding et al., 2012; Ma et al., 2018; Zhu et al., 2014; Miao et al., 2015; Xu et al., 2009, 2010; Kurtén et al., 2014).

The pioneering laboratory experiments about nucleation of organic acids and many theoretical studies have clearly shown that organic acids promote the growth of nanoparticles (Han et al., 2018; Nadykto and Yu, 2007; Zhang et al., 2004; Zhao et al., 2006, 2009). The interactions between five dicarboxylic acids and sulfuric acid have been studied by Zhang group (Xu and Zhang, 2012). Among them, oxalic acid is a most prevalent dicarboxylic acid in the atmosphere and a major constituent of aerosol particles (Limbeck et al., 2001; Chebbi and Carlier, 1996; Martinelango et al., 2007; Huang et al., 2005; Zobrist et al., 2006). Oxalic acid has been shown that it could contribute to the aerosol nucleation process by binding to sulfuric acid and ammonia (Xu and Zhang, 2012). The theoretical investigation of Yu et al. predicted that oxalic acid significantly enhances the stability of ionic clusters and catalyzes pre-nucleation clusters with positive charges (Xu et al., 2010). Moreover, Tao et al. reported that thermodynamically stable $C_2H_2O_4$–NH_3 core clusters could participate in NPF events (Weber et al., 2012). The interaction between oxalic acid and dimethylamine is strongly dependent on the degree of hydration of the acid and dimethylamine (Chen et al., 2017a). While nucleation of dicarboxylic acids have been extensively studied in the past, role of monocarboxylic acids in atmospheric nucleation is yet to be understood, In this study, the role of monocarboxylic acetic acid, one of the most abundant organic species in the atmosphere has been investigated (Andreae et al., 1988; Galloway et al., 1982). For example, in the Amazonia region of Brazil, the average concentration of gas-phase acetic acid is 2.2 ± 1.0 ppb and it is about 2 orders of magnitude higher than that of the other corresponding organic acids in the atmospheric aerosol (Andreae et al., 1988). In Denmark, the formic acids and acetic acids account for $18\% \pm 8\%$ of the total acids in rain (Granby et al., 1997). In Austria, the most abundant Carboxy acids were acetic (average: 0.93 $\mu g\, ml^{-1}$) at a continental background site (Löflund et al., 2002). Nadykto et al. indicated that common low-molecular acetic acids considerably promote new particle formation (Nadykto and Yu, 2007). Besides, acetic acids could efficiently stabilize small sulfuric acid–water complexes and can also interact actively with ammonia (Nadykto and Yu, 2007). In particular, hydration of (HOAc) $(SA)_2$ has a profound impact on ion-mediated nucleation (Zhu et al., 2014). Despite the abundance of HOAc, the atmospheric property of acetic acids is poorly understood. In particular, the contribution of acetic acids and strong bases to atmospheric nucleation remains unknown.

Laboratory studies and recent field observations have reported that amines are involved in new particle formation (Smith et al., 2010; Zhao et al., 2011; Almeida et al., 2013). Dimethylamine (DMA), the most common and strongest organic base in the atmosphere, promotes neutral and ion-induced sulfuric acid–water nucleation (Ge et al., 2011; Jen et al., 2014). Experiments using the CLOUD chamber at CERN have indicated that the concentration of DMA is exceeding three parts per trillion by volume, and it has a much higher nucleation rate than ammonia in the atmosphere (Almeida et al., 2013).

According to previous studies, both HOAc and DMA are involved in NPF events, however, impacts of the interaction of HOAc and DMA have not been investigated. In this study, structures and thermodynamics of the (HOAc) (DMA) (H2O)n (n = 0–4) are studied by PW91PW91/6–311++G (3df, 3pd) level. Topological analysis, atmospheric relevance, the formation rates and evaporation rates of the (HOAc) (DMA) $(H_2O)_n$ (n = 0–4) clusters are also explored.

2. Methods

The low energy structures of (HOAc) $(H_2O)_n$ (n = 1–4) and (HOAc) (DMA) $(H_2O)_n$ (n = 0–4) clusters were obtained using the Basin-Hopping (BH) algorithm coupled with semiempirical PM7 implemented in MOPAC 2016 (Hostaš et al., 2013; Wales and Doye, 1997; Huang et al., 2010; Maia et al., 2012). To obtain the low-lying structures with the BH method, two steps were needed: firstly, new configuration was generated through the random displacement of molecules in the cluster; and then, the structure was optimized to the local minimum by PM7 method. Secondly, Boltzmann temperature was set to range from 2000 to 5000 K in this study, and the energy of optimized local minimum was used as the criteria to accept or reject the initial structures by Metropolis guidelines (Chen et al., 2017b; Zhao et al., 2017; Jiang et al., 2014). For each size cluster, ten separate BH searching were performed and each searching contained 500 sampling structures at the Boltzmann temperature. Then, the energy was sorted from low to high and 30 low energy geometries relative to global minimum were selected to be optimized (Liu et al., 2014; Wen et al., 2018). The initial geometries of (HOAc) $(H_2O)_n$ (n = 1–4) and (HOAc) (DMA) $(H_2O)_n$ (n = 0–4) were first optimized at the PW91PW91/6-31 + G* level. After that, the stable isomers within 6 kcal mol^{-1} were further optimized at the PW91PW91/6–311++G (3df, 3pd) level to determine the final geometries (Peng et al., 2015; Wang et al., 2018). Cartesian geometries of global minima are given in the Supporting Information. For each stationary point, the vibration frequency is calculated to confirm that no imaginary frequencies were present. All the geometry optimizations and frequency calculations were implemented by Gaussian 09 program (Frisch et al., 2004).

Nadykto et al. (Nadykto and Yu, 2007) indicated that the comparison between theoretical results and the experimental data shows that PW91PW91/6–311++G (3df, 3pd) over-performs both MP2/6–311++G (3df, 3pd) and B3LYP/6–311++G (3df, 3pd) in the study of strong hydrogen bonding between atmospheric nucleation precursors and common organics. PW91PW91 functional was selected as the specific method in this study, due to its fine performance in obtaining stable structures, thermochemistry, and non-covalent interactions (NCI) for different atmospheric clusters, and its predictions are highly similar to the experimental results (Xu et al., 2009, 2010; Xu and Zhang, 2012). Meanwhile, the 6–311++G (3df, 3pd) basis set was selected due to its wide applications in atmospheric clusters (Nadykto and Yu, 2007; Nadykto et al., 2008b; Miao et al., 2015).

To elucidate the non-covalent interactions (NCI) of the clusters, we implemented it in Multiwfn 3.0[79] and visualized it by the visual molecular dynamics (VMD) program (Humphrey et al., 1996), which has been certified to be effective and convenient for identifying NCI. In addition, the results from the quantum chemistry calculations were implemented in a dynamics model to simulate the kinetics of molecular cluster populations (McGrath et al., 2012), and we can also study the formation rates and the evaporation rates of the (HOAc) (DMA) $(H_2O)_n$ (n = 0–4) clusters. The Atmospheric Cluster Dynamics Code (ACDC) simulation was operated at 298.15 K. The HOAc concentration and the DMA concentration were set to 5×10^{10} molecule cm^{-3} and 5 ppt, respectively (Andreae et al., 1988; Almeida et al., 2013). The relative humidity (RH) in the study of formation rate is set to 0–100%, and the hydration effect on evaporation rates is also considered.

3. Results and discussion

3.1. Structure

The geometries of (HOAc) $(H_2O)_n$ (n = 1–4) and (HOAc) (DMA) $(H_2O)_n$ (n = 0–4) were optimized at PW91PW91/6–311++G (3df, 3pd) level, shown in Fig. 1 and Fig. 2. All the low-energy structures are listed in the Supporting Information. The Gibbs free energies of the structures are ordered by a<b < c < d < e. The representations of these structures

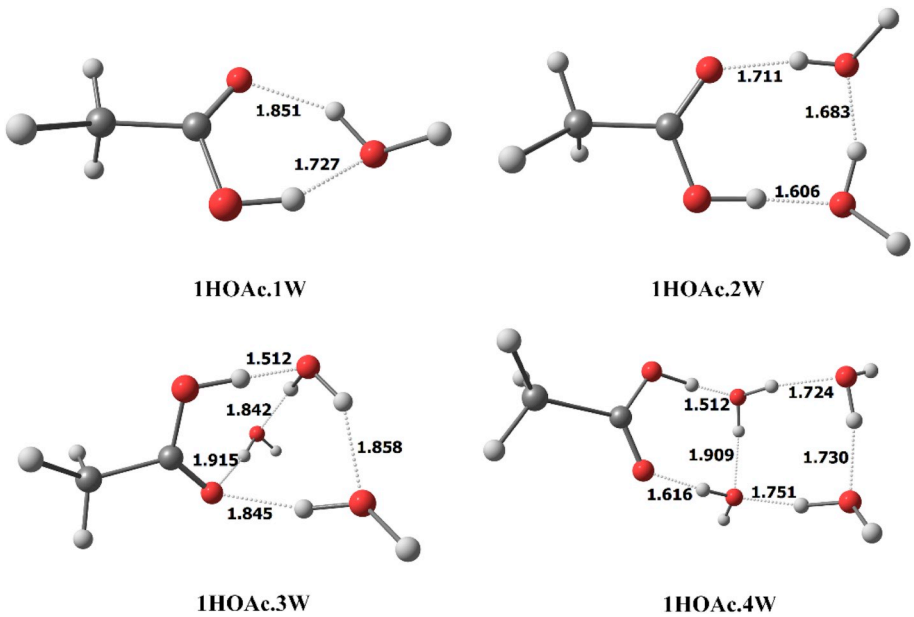

Fig. 1. Global minima of (HOAc) $(H_2O)_n$ (n = 1–4) calculated at the PW91PW91/6–311++G (3df, 3pd) level.

are defined using n-i notation. In this notation, "n" (n = 0–4) represents the number of water molecules. "i" (i = a-e), denotes different isomers with the same value of n.

For (HOAc) $(H_2O)_n$ (n = 1–4), the optimized global minimum structures are presented in Fig. 1. For monohydrated clusters, there are two hydrogen bonds between water and the acetic. The distance of hydrogen bond between the acetic OH group and the oxygen in water is 1.727 Å. In the case of dehydrate of acetic acid, a three-membered ring is formed through the two water molecules and acetic acid, and it is made up of three hydrogen bonds, with the length of 1.606 Å, 1.683 Å and 1.711 Å, successively. In this cluster, the strength of hydrogen bond between the acetic acid and water appears to be higher than that of monohydrate. In the case of the trihydrate global minimum, there are five O···H hydrogen bonds in the lowest energy configuration. In the five hydrogen bonds of this cluster, the hydrogen bond between acetic acid and the oxygen in water of 1.512 Å appears to be the shortest one. It is obvious that, when adding the third and the fourth water to acetic, water molecules begin to form O···H hydrogen bond with themselves, which may be caused by space steric effect. With the increasing number of water molecules, the clusters gradually form more stable three-dimensional structures.

Optimized structures of global minima of (DMA) (HOAc) (H2O)n (n = 0–4) clusters are presented in Fig. 2. For (HOAc) (DMA) dimer, the most stable structure has one hydrogen bond, with the length of 1.625 Å between the amino group and carboxyl group. For the most stable structure of (HOAc) (DMA) $(H_2O)_1$, one hydrogen bond is formed between the acid group and the nitrogen of dimethylamine, with a distance of 1.468 Å. For the most stable structure of (HOAc) (DMA) $(H_2O)_n$ (n = 2–4), proton transfer from acetic acid to dimethylamine occurs. For the (HOAc) (DMA) $(H_2O)_2$ cluster, a four-membered ring is formed through two water molecules, acetic acid and dimethylamine, which is composed of four O···H hydrogen bonds, with the length of 1.347 Å, 1.600 Å, 1.631 Å and 1.760 Å, successively. As the number of water increases up to three, the most stable one has two adjacent cyclic hydrogen bonded networks, and the distance of OH hydrogen bond between the acid groups and the nitrogen of dimethylamine is 1.476 Å. Besides, the water molecules begin to form OH···O hydrogen bond with themselves. For (HOAc) (DMA) $(H_2O)_4$, the most stable structure has a stable quasi-cubic configuration.

The addition of DMA can promote the formation of intermolecular hydrogen bond in the cluster, because the presence of DMA provides more the sites of hydrogen bond, and the addition of DMA enables itself to act as a receptor for proton transfer with HOAc, which makes the occurrence of the intermolecular hydrogen bond in HOAc-DMA is easier than that of HOAc-H_2O. The carboxyl group is directly connected to the amino group in all the most stable configurations. When adding two or more water molecules, proton transfer from HOAc to DMA occurs in clusters. Proton transfer enhances the strength of hydrogen bond as well as promotes the generation of global minimum structures.

3.2. Thermochemical analysis

Thermodynamic analysis of the global minimum of (HOAc) $(H_2O)_n$ (n = 1–4), (DMA) $(H_2O)_n$ (n = 1–4) and (HOAc) (DMA) $(H_2O)_n$ (n = 0–4) was carried out by PW91PW91/6–311++G (3df, 3pd) level. The relative single-point energy, △E (0 K), is obtained by two main reaction paths, as shown in equations (1) and (2): $\triangle E_1$ is calculated by adding a single molecule, and $\triangle E_2$ is calculated by adding water to the acid-base dimer, the other paths are placed in path S1and path S2 in SI. The intermolecular enthalpy △H (298.15 K) and the Gibbs free energy △G (298.15 K) are also calculated by those two ways. The thermodynamic analysis of the global minimum for (HOAc) $(H_2O)_n$ (n = 1–4), (DMA) $(H_2O)_n$ (n = 1–4) and (HOAc) (DMA) $(H_2O)_n$ (n = 0–4) is listed in Tables 1 and 2.

$$\text{path1}: \quad \Delta E_1 = E_{(HOAc)(DMA)(H_2O)_n} - E_{(HOAc)} - E_{(DMA)} - nE_{(H_2O)} \tag{1}$$

$$\text{path2}: \quad \Delta E_2 = E_{(HOAc)(DMA)(H_2O)_n} - E_{(HOAc)(DMA)} - nE_{(H_2O)} \tag{2}$$

The △G values of (HOAc) $(H_2O)_n$ (n = 1–4) and (DMA) $(H_2O)_n$ (n = 1–4) are summarized in Table 1, and almost all the △G values are positive except for (HOAc) $(H_2O)_1$, which has a value of -0.47 kcal mol^{-1}, indicating the (HOAc) $(H_2O)_1$ could spontaneously form in the atmosphere. It may be deduced from Table 1 that (HOAc) $(H_2O)_n$ (n = 2–4) and (DMA) $(H_2O)_n$ (n = 1–4) clusters could not be favorable in the atmosphere.

When HOAc interacts with DMA, the △G value turns to be negative, which is -3.48 kcal mol^{-1}. In path 1, the △G value of (HOAc) (DMA) $(H_2O)_1$ is -4.61 kcal mol^{-1}, which is 4.14 kcal mol^{-1} less than that of (HOAc) $(H_2O)_1$, while the △G values of the (HOAc) (DMA) $(H_2O)_2$, (HOAc) (DMA) $(H_2O)_3$, (HOAc) (DMA) $(H_2O)_4$ are -3.33 kcal mol^{-1}, -2.62 kcal mol^{-1} and -1.08 kcal mol^{-1}, respectively. The △G values of the Ternary clusters are lower than the acetic hydrate. With the addition

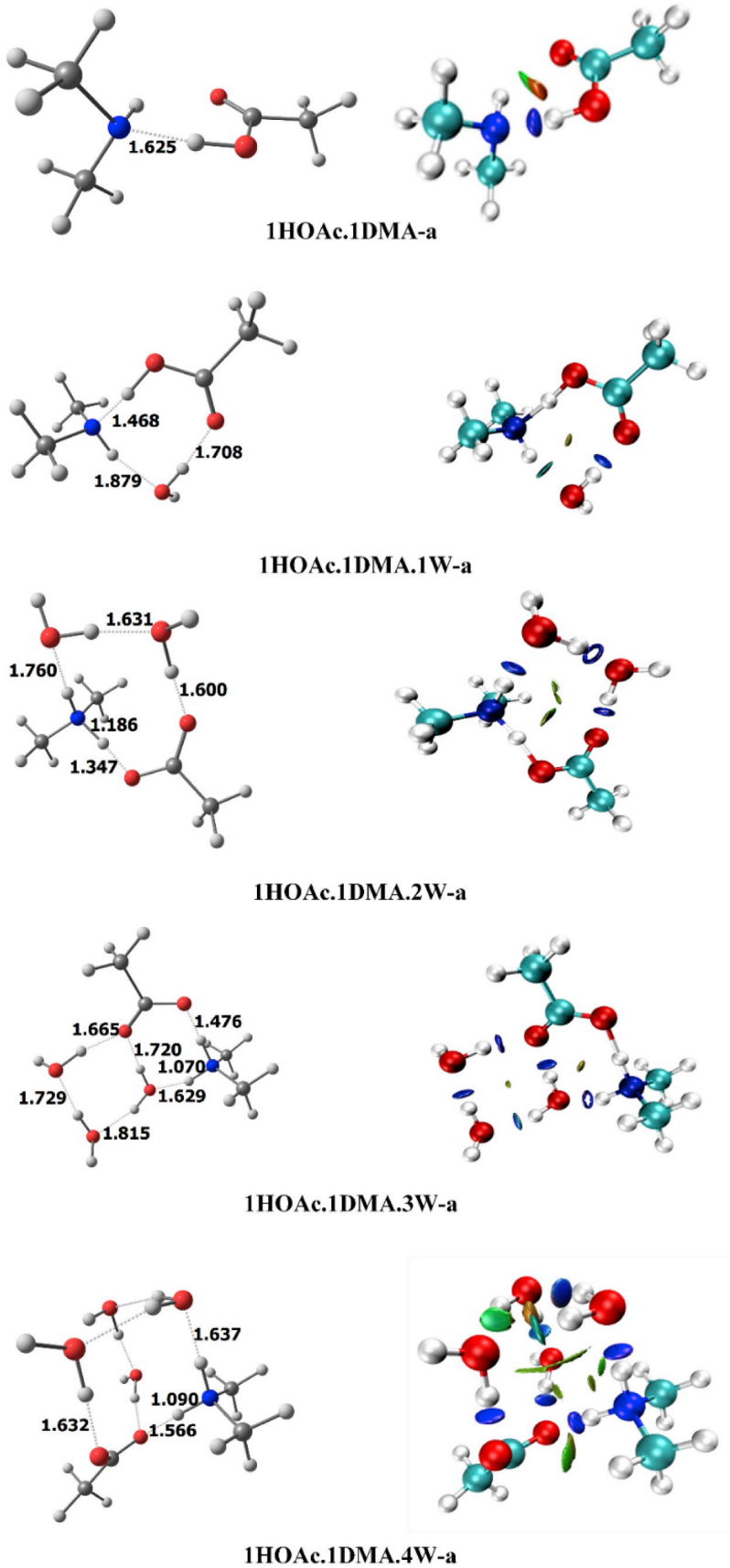

Fig. 2. Global minima of (HOAc) (DMA) $(H2O)_n$ (n = 0–4) calculated at the PW91PW91/6–311++G (3df, 3pd) level. The intramolecular and intermolecular interaction distances and the corresponding isosurfaces are given.

Table 1
Energy changes associated with the reaction of (HOAc) $(H_2O)_n$ (n = 1–4) and (DMA) $(H_2O)_n$ (n = 1–4). The energies are in kcal mol^{-1}, and were calculated at the PW91PW91/6–311++G (3df, 3pd) level.

Reaction	△E (0 K)	△H (298.15 K)	△G (298.15 K)
HOAc + H_2O ↔ (HOAc) (H_2O)	−9.77	−10.08	−0.47
HOAc + $2H_2O$ ↔(HOAc) $(H_2O)_2$	−17.45	−20.85	0.97
HOAc + $3H_2O$ ↔(HOAc) $(H_2O)_3$	−21.70	−27.57	3.34
HOAc + $4H_2O$ ↔(HOAc) $(H_2O)_4$	−22.76	−31.28	6.06
DMA + H_2O ↔ (DMA) (H_2O)	−4.16	−6.63	0.79
DMA + $2H_2O$ ↔(DMA) $(H_2O)_2$	−9.66	−15.37	2.25
DMA + $3H_2O$ ↔(DMA) $(H_2O)_3$	−13.43	−22.61	4.23
DMA + $4H_2O$ ↔(DMA) $(H_2O)_4$	−20.10	−32.44	5.23

Table 2
Energy changes are associated with the formation of (HOAc) (DMA) $(H_2O)_n$ (n = 0–4). The energies are in kcal mol^{-1}, and were calculated at the PW91PW91/6–311++G (3df, 3pd) level.

Reaction	△E (0 K)	△H (298.15 K)	△G (298.15 K)
HOAc + DMA↔ (HOAc) (DMA)	−14.24	−12.25	−3.48
HOAc + DMA + H_2O ↔ (HOAc) (DMA) (H_2O)	−23.24	−23.35	−4.61
(HOAc) (DMA)+H_2O↔ (HOAc) (DMA) (H_2O)	−9.00	−11.10	−1.17
HOAc + DMA+$2H_2O$↔(HOAc) (DMA) $(H_2O)_2$	−28.86	−31.99	−3.33
(HOAc) (DMA)+$2H_2O$↔ (HOAc) (DMA) $(H_2O)_2$	−13.73	−16.02	−3.99
HOAc + DMA +$3H_2O$ ↔ (HOAc) (DMA) $(H_2O)_3$	−34.07	−41.89	−2.62
(HOAc) (DMA)+$3H_2O$↔ (HOAc) (DMA) $(H_2O)_3$	−13.00	−15.04	−7.18
HOAc + DMA + $4H_2O$ ↔ (HOAc) (DMA) $(H_2O)_4$	−37.69	−47.07	−1.08
(HOAc) (DMA)+$4H_2O$↔ (HOAc) (DMA) $(H_2O)_4$	−8.43	−8.49	−6.66

of water molecules, clusters are less likely in the atmosphere. In path 2, the △G value of (HOAc) (DMA) $(H_2O)_3$ shows the most negative value (−7.18 kcal mol^{-1}), indicating that the clusters constructed by three waters and the acid-base dimer could be more favorable than other clusters in the atmosphere.

When adding the DMA to (HOAc) $(H_2O)_n$ (n = 1–4), the △G values become lower. DMA facilitates the progress of the reaction and increases the stability of the clusters, which is consistent with the structural analysis and temperature dependence analysis in later depictions.

3.3. Analysis of the topological parameters and the non-covalent interaction (NCI)

The topological parameters and the NCI of the global minimum of (HOAc) (DMA) $(H_2O)_n$ (n = 0–4) will be discussed in this section. In order to explore the nature of the hydrogen bonds on the stability of the global minimum structures, the "atoms in molecules" (AIM) theory of Bader is used to analyze the characteristics of bond critical points (BCPs) in H–N···H···O (Han et al., 2018; Bader, 1990; Carroll et al., 1988; Gao et al., 2013; Bone and Bader, 1996; Rozas et al., 2000). To analyze the topological characteristics at the bond critical point, we study five parameters: the electron density (ρ), its Laplacian ($\triangle^2\rho$), the electronic kinetic energy density (G) and the electronic potential energy density (V), with the latter two composing the third one, the electronic energy density (H). One of the most important parameters is the electron density, which reveals the existence of the electron density redistribution at hydrogen bond. All of the topological parameters at BCPs of the N···H bonds and O···H hydrogen bonds are presented in Table 3, including the length of hydrogen bonds calculated at the PW91PW91/6–311++G (3df, 3pd) level, and the gradient isosurfaces display a vivid visualization of strength of NCI in the right half of Fig. 2. Both the topological analysis of AIM theory and the analysis of the NCI were carried out by Multiwfn program (Contreras-García et al., 2011) and VMD (Humphrey et al., 1996) program.

As the number of water molecules in (HOAc) (DMA) $(H_2O)_n$ increases from one to two, the length of H–N···H bond quickly decreases from 1.468 Å to 1.186 Å, while the electronic density value sharply increases from 0.1038 a.u. to 0.2180 a.u, which means the strength of the hydrogen bond increases. It has been known that the larger the electronic density is, the stronger the hydrogen bond is (Galvez et al., 2003). In (HOAc) (DMA) $(H_2O)_2$, proton transfer from the oxygen atom of HOAc to the nitrogen atom of DMA occurs, indicating the second water triggers the proton transfer. However, when adding the second water to (HOAc) (H2O), no proton transfer occurs. This indicates that the presence of DMA plays important role in proton transfer.

The strength of hydrogen bond can be classified by the value of $\triangle^2\rho$ and H. When both $\triangle^2\rho$ and H are negative, hydrogen bond is strong. When $\triangle^2\rho$ is positive and H is negative, it is regarded as medium hydrogen bond. When both $\triangle^2\rho$ and H are positive, the hydrogen bond is weak (Rozas et al., 2000). The$\triangle^2\rho$ value is used to distinguish covalent or non-covalent interactions. Generally, when the$\triangle^2\rho$ value is negative, it represents the covalent bond; when the $\triangle^2\rho$ value is positive, it means the non-covalent bond (Han et al., 2018; Kim et al., 1994). Therefore, these criteria are used to characterize different hydrogen bonds in the global minima of (HOAc) (DMA) $(H_2O)_n$ (n = 0–4). For (HOAc) (DMA) and (HOAc) (DMA) $(H_2O)_1$ clusters, $\triangle^2\rho > 0$ and $H < 0$ suggest medium hydrogen bonds. For (HOAc) (DMA) $(H_2O)_n$ (n = 2–4) clusters, both $\triangle^2\rho$ and H are negative, indicating strong hydrogen bonds in the closed-shell interactions.

The reduced gradient isosurfaces (s = 0.05 a.u.) are displayed in the right half of Fig. 2. The NCI analysis method can be seen as an extension of AIM, and the reduced density gradient is able to be used to confirm non-covalent interactions and covalent interactions in real space. Blue color represents hydrogen bonds; green represents van der Waals forces; and red means steric hindrance. The darker the corresponding color is, the stronger the interaction is. For (HOAc) (DMA) and (HOAc) (DMA) $(H_2O)_1$, the blue color at N···H bond represents the hydrogen bonds. For (HOAc) (DMA) $(H_2O)_n$ (n = 2–4), acid and base are directly connected by NH···O bond, which could be explained by the proton transfer according to the AIM results.

3.4. Temperature dependence of conformational populations

In previous studies, it was shown that the thermodynamic properties

Table 3
N···H distances (Å) and topological parameters at intermolecular and intramolecular bond critical points (BCPs) of the H–N···H···O bonds in the global minima of (HOAc) (DMA) $(H_2O)_n$ (n = 0–4) calculated at the PW91PW91/6–311++G (3df, 3pd) level.

n	D (N…HO) /Å	ρ /a.u.	G /a.u.	V /a.u.	H /a.u.	$\triangle^2\rho$ /a.u.	-G/V
0	1.625	0.0696	0.0394	−0.0667	−0.0273	0.0484	0.5907
1	1.468	0.1038	0.0485	−0.1066	−0.0581	0.0385	0.4550
2	1.186	0.2180	0.0553	−0.3133	−0.2580	−0.8107	0.1765
3	1.070	0.2626	0.0516	−0.4146	−0.3630	−1.2458	0.1245
4	1.090	0.2869	0.0499	−0.4694	−0.4195	−1.4787	0.1063

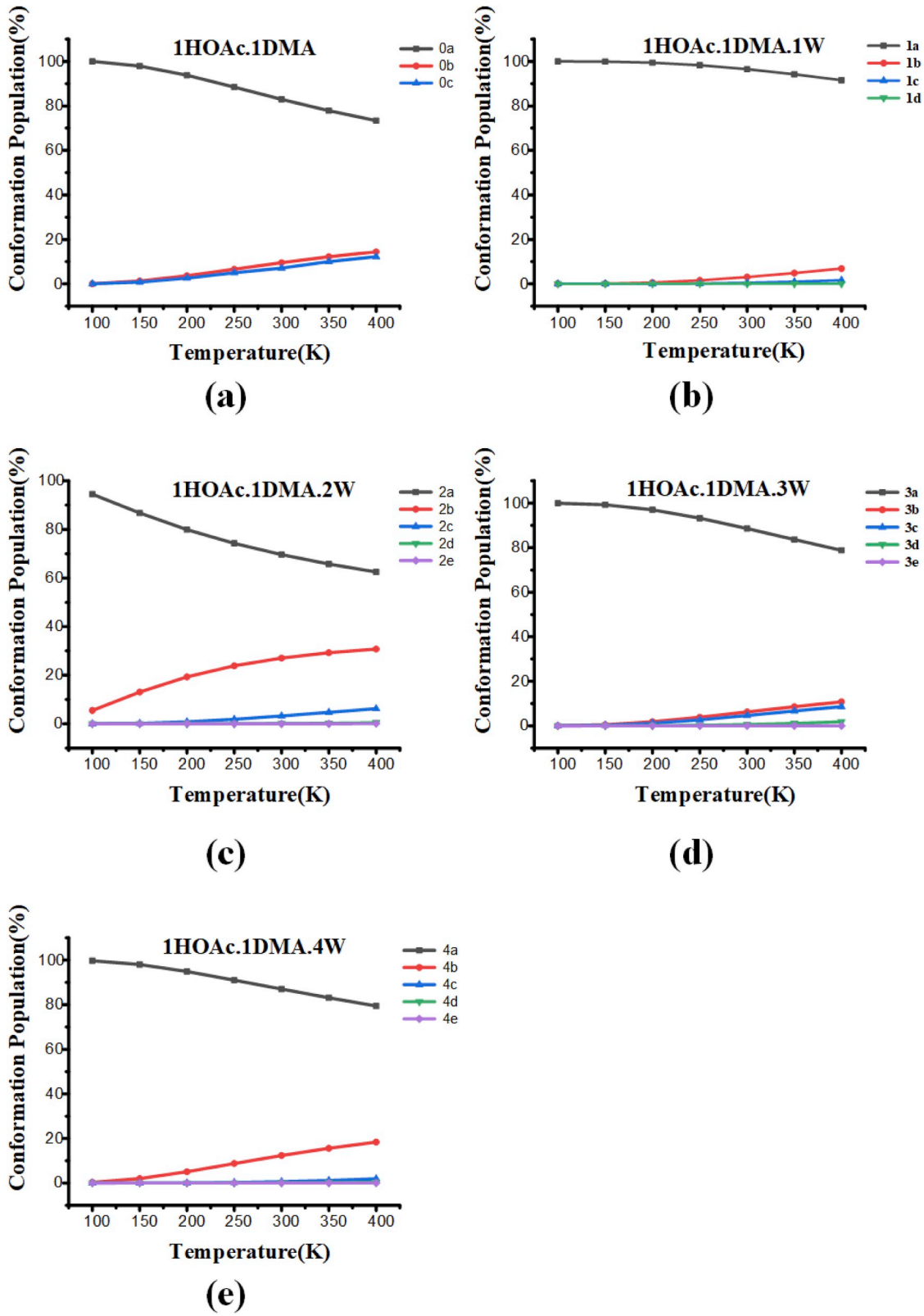

Fig. 3. Conformational population changes vs. temperature for the low-energy isomers of (HOAc) (DMA) $(H_2O)_n$ (n = 0–4) calculated at the PW91PW91/6–311++G (3df, 3pd) level.

of clusters depend on temperature, which in turn affects the order of the conformational populations (Han et al., 2018; Miao et al., 2015; Mhin et al., 1993). Therefore, it is important to investigate the effect of temperature on the formation of (HOAc) (DMA) $(H_2O)_n$ (n = 0–4) clusters. However, it is hard to complete experiments under low temperature conditions, due to the increasing wall losses of the clusters. Fortunately, theoretical calculation can be used to predict possible results.

The changes in Gibbs free energy with temperatures from 100 to

400 K could have a large influence on the relative populations of different isomers. Thus, an effect of temperature on the relative populations of different isomers with the same size is needed to explore. The relative conformation population is defined by:

$$p_i = \exp(-\Delta\Delta G_i / RT) \Big/ \sum_i \exp(-\Delta\Delta G_i / RT) \quad (3)$$

In equation (3): R is the ideal gas constant, T represents the temperature, pi means the relative population of the ith isomer at one cluster size, $\triangle\triangle G_i$ represents the Gibbs free energy of the ith isomer compared to the most stable one.

For (HOAc) (DMA) (Fig. 3(a)) dimer, our results predict a very sharp decrease in the proportion of 0a from practically 100%–73.4% with the increasing temperature, the proportions of isomer-b and isomer-c increase slightly. For monohydrate (Fig. 3(b)), 1a is the most prevalent conformer with a share of 100 percent at 100 K. As temperature increasing to 400 k, 1a still plays a dominant role with a proportion of 91.6%. As a comparison, 1 b only has a proportion of 6.8%, and the sum of the weight of 1a and 1 b almost reaches 1. In the process, other isomers are negligible. In (HOAc) (DMA) $(H_2O)_2$ (Fig. 3(c)), the most prevalent conformer is 2a, dropping significantly from 94.5% to 62.5% as the temperature increases in the range of 100–400 K. When the temperature reaches 400 K, the proportions of 2 b and 2c are approximately 30.7% and 6.2%, respectively.

For (HOAc) (DMA) $(H_2O)_3$ (Fig. 3(d)), the proportion of 3a steadily decreases from 99.9% to 77.8% in the range of 100–400 K. The isomers of 3 b and 3c have similar trends. For the n = 4 (Fig. 3(e)), 4a weighs more than other low-lying isomers as temperature changes. However, the weight of following 4 b cannot be ignored, which increases significantly in the range of 100–400 K.

In conclusion, it is crucial to understand how a specific nucleation mechanism works at different temperatures. As the temperature rises, the weight of the global minima decreases while that of other local minimum increase. Kim et al. indicated that it is easy to change the stabilities of the clusters containing multiple hydrogen bonds when the temperature rises, which is a result of the entropy effect (Kim et al., 1994), and it may explain the phenomenon that the strong temperature dependence for (HOAc) (DMA) $(H_2O)_n$ (n = 0–4).

3.5. Atmospheric relevance and parameters in kinetic code

Previous studies (Han et al., 2018; Xu and Zhang, 2013) have shown that hydration plays a vital role in the nucleation of amines and organic acids. In order to explore what kind of clusters is dominating at a certain relative humidity (RH), the results of the hydrate distributions of the "core (HOAc) (DMA) at four different RHs (20%, 50%, 80%, 100%) with a temperature of 298.15 K are revealed. As an n-hydrate in this study, its relative concentration is defined by:

$$\frac{\rho(1,m)}{\rho^{total}_{HOAc-DMA}} = \frac{\rho(1,m)}{\rho(1,0)+\rho(1,1)+\ldots+\rho(1,n)} = \frac{K_1K_2\ldots\left(S\frac{P^{eq}_W}{P}\right)^m}{1+K_1S\frac{P^{eq}_W}{P}+\ldots+K_1K_2\ldots K_n\left(S\frac{P^{eq}_W}{P}\right)^n} \quad (4)$$

In equation (4), K_n are the equilibrium constants, related to the formation energy of an n-hydrate formed from one water molecule and (n-1)-hydrate (Loukonen et al., 2010). ρ represents the concentration of different species, and S is the saturation ratio, which is defined as the ratio of the proper partial pressure of the water vapor to the saturation vapor pressure P^{eq}_W (Loukonen et al., 2010; Noppel et al., 2002). Besides, relative humidity is defined as RH = 100% × S, and the reference pressure (P) is 1 atm (Miao et al., 2015; Temelso et al., 2012).

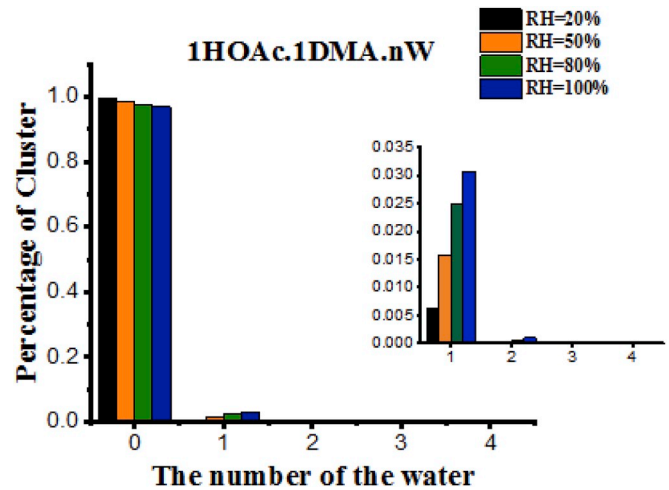

Fig. 4. Hydrate distributions of (HOAc) (DMA) $(H_2O)_n$ (n = 0–4) clusters at the temperature of 298.15 K.

As illustrated in Fig. 4, the non-hydrated cluster is always dominant, the monohydrate and the dihydrate account for a small proportion, and the trihydrate and tetrahydrate are practically nonexistent. As the RH increases from 20% to 100%, the non-hydrated decreased slightly from 99% to 96%, while the monohydrate is virtually increased from 0.6% to 3%. In conclusion, the sensitivity of the hydrate distributions of (HOAc) (DMA)clusters to relative humidity is negligible, and the non-hydrated cluster dominates all the time.

The formation rate of clusters is a crucial parameter in the NPF (Chen et al., 2012; Wen et al., 2019). Fig. 5(a) shows the cluster formation rates (J_{calc}) as a function of relative humidity (RH: ranging from 0 to 100%) for HOAc concentration is 5×10^{10} molecule cm^{-3} (Andreae et al., 1988), DMA concentration is 5 ppt (Almeida et al., 2013), and the temperature is 298.15 K. Generally, the cluster formation rate decreases with the increasing RH for the considered conditions. When the RH<25%, the simulated cluster formation rate J_{calc} decreases rapidly, indicating that the cluster formation rate is significantly reduced by the hydration environment. Whereas for the RH >25%, the J_{calc} decreases slowly compared to the values when RH <25%, indicating that 25% RH is a turning point. It is worth noting that the cluster formation rate J_{calc} is $9.98 \times 10^6\ cm^{-3}\ s^{-1}$ at RH = 25%, which is around the usual experimental humidity (Wen et al., 2019). The result is consistent with the conclusion in atmospheric relevance that non-hydrated clusters have the high proportion at low relative humidity.

Recently, the evaporation rates of clusters based on the formation free energy have been identified to be a meaningful parameter to study the early stage of particle formation (Ortega et al., 2012; McGrath et al., 2012). In terms of magnitude of the evaporation rate, the data in Fig. 5 (b) is comparable to our previous study (Chen et al., 2017a; Wen et al., 2018).

In Fig. 5(b), the evaporation of H_2O is larger than the evaporation of HOAc and DMA, because proton transfer from HOAc to DMA is

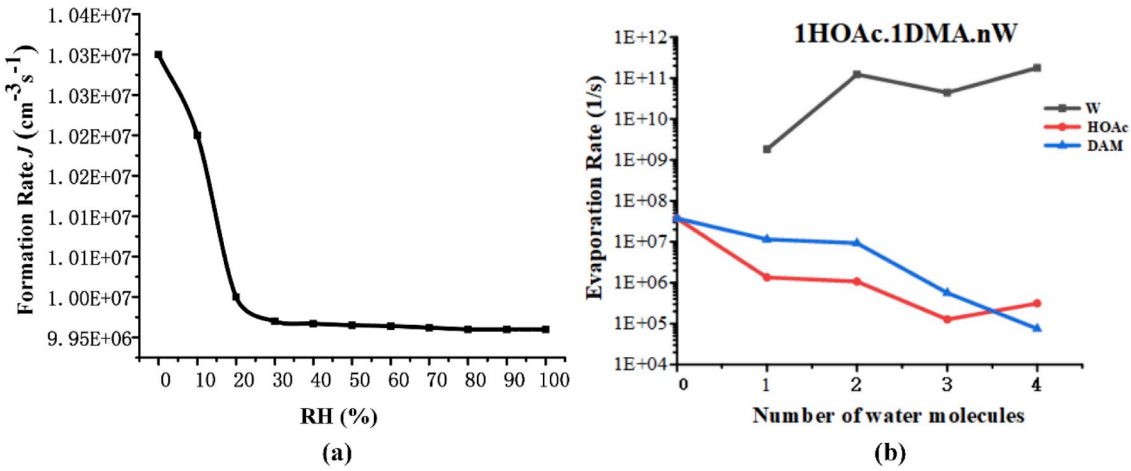

Fig. 5. (a) Simulating formation rates J_{calc} (cm^{-3} s^{-1}) as a function of relative humidity (RH) at 298.15 K, HOAc concentration (5×10^{10} molecule cm^{-3}), and DMA concentration (5 ppt). (b) Evaporation rates of HOAc, DMA and H_2O from (HOAc) (DMA) $(H_2O)_n$ (n = 0–4) clusters.

significant in stabilizing the acid-base cluster. And hydration can decrease the evaporation rates of HOAc and DMA, because the participation of water promotes the proton transfer from HOAc to DMA. The result is consistent with the analysis about structures of the clusters. In this study, it is clear that the evaporation rates are dependent on the △G value, so the accuracy about the calculation of △G value is very important and worthwhile to obtain more accurate kinetic data in the further studies.

4. Conclusions

In this study, the nucleation mechanisms of (HOAc) $(H_2O)_n$ (n = 1–4) and (HOAc) (DMA) $(H_2O)_n$ (n = 0–4) are theoretically investigated by PW91PW91/6–311++G (3df, 3pd) level. Structures, thermodynamic analysis, topological parameters, temperature effect, atmospheric relevance, formation rates and evaporation rates of the clusters are explored.

In (HOAc) (DMA) $(H_2O)_n$ (n = 2–4) clusters, proton transfer from HOAc to DMA occurs. Proton transfer enhances the strength of hydrogen bond as well as promotes the generation of global minimum structure. The analyses of the electron density and noncovalent interactions reveal that intermolecular hydrogen bond plays a significant role in (HOAc) (DMA) $(H_2O)_n$ (n = 0–4) clusters. In addition, through the previous studies, we conclude that the synergistic effect of HOAc and DMA might enhance the stability of clusters containing sulfuric acid.

The relative populations of different isomers within the same cluster size at various temperatures from 100 K to 400 K show that the weight of the global minimum decreases but that of other local minima increase, and all the isomers contribute to the nucleation of clusters. The non-hydrated clusters are always dominant. With higher RH, the percentage of non-hydrated clusters decreases slightly, and the RH effect on the hydrate distributions of (HOAc) (DMA) clusters is negligible. Through the studies of the formation rates and evaporation rates of the clusters, it was confirmed that the nucleation ability of the HOAc-DMA clusters is relatively strong, and the non-hydrated clusters prefer to existing in low humidity environment. In addition, hydration could decrease the evaporation rates of HOAc and DMA.

While our work provides a starting point for further studies of atmospheric nucleation involving acetic acid, dimethylamine and water, there exist a number of questions yet to be answered. For example, it is still unclear how HOAc reacts with other atmospheric nucleation precursors in the presence of dimethylamine and water. Further field observations, theoretical calculations and experimental studies are required to investigate the possible reactions under atmospheric condition.

Declaration of competing interest

The authors declare that they have no known competing financial interests or personal relationships that could have appeared to influence the work reported in this paper.

Acknowledgements

This work was supported by the National Natural Science Foundation of China (Grant No. 21573241, 41605099, 41705097, 41705111, 41775112 and 41527808), the National Science Fund for Distinguished Young Scholars (Grant No. 41725019), Key Research Program of Frontier Science, CAS (Grant No. QYZDB-SSW-DQC031), The Key Research Program of the Chinese Academy of Sciences (Grant No. ZDRW-ZS-2016-4-3-6), the National Key Research and Development Program (Grant No. 2016YFC0202203 and 2016YFC0202703) and National Research Program for Key Issues in Air Pollution Control (DQGG0103).

Appendix A. Supplementary data

Supplementary data to this article can be found online at https://doi.org/10.1016/j.atmosenv.2019.117005.

References

Almeida, J., Schobesberger, S., Kürten, A., Ortega, I.K., Kupiainen-Määttä, O., Praplan, A. P., Adamov, A., Amorim, A., Bianchi, F., Breitenlechner, M., 2013. Molecular understanding of sulphuric acid–amine particle nucleation in the atmosphere. Nature 502 (7471), 359.

Andreae, M., Talbot, R., Andreae, T., Harriss, R., 1988. Formic and acetic acid over the central Amazon region, Brazil: 1. Dry season. J. Geophys. Res.: Atmos. 93 (D2), 1616–1624.

Bader, R., 1990. Atoms in Molecules: A Quantum Theory. Oxford Univ. Press, Oxford.

Baker, M.B., Peter, T., 2008. Small-scale cloud processes and climate. Nature 451 (7176), 299.

Bone, R.G., Bader, R.F., 1996. Identifying and analyzing intermolecular bonding interactions in van der Waals molecules. J. Phys. Chem. 100 (26), 10892–10911.

Bork, N., Kurtén, T., Enghoff, M., Pedersen, J.O.P., Mikkelsen, K.V., Svensmark, H., 2011. Ab initio studies of $O_2^-(H_2O)_n$ and $O_3^-(H_2O)_n$ anionic molecular clusters, n≤ 12. Atmos. Chem. Phys. 11 (14), 7133–7142.

Bork, N.C., Kurtén, T., Enghoff, M.A.B., Pedersen, J.O.P., Mikkelsen, K., Svensmark, H., 2011. Structures and reaction rates of the gaseous oxidation of SO2 by an O− 3 $(H_2O)_{0-5}$ cluster–a density functional theory investigation. Atmos. Chem. Phys. Discuss. 11, 29647–29679.

Bzdek, B.R., Pennington, M.R., Johnston, M.V., 2012. Single particle chemical analysis of ambient ultrafine aerosol: a review. J. Aerosol Sci. 52, 109–120.

Carroll, M.T., Chang, C., Bader, R.F., 1988. Prediction of the structures of hydrogen-bonded complexes using the Laplacian of the charge density. Mol. Phys. 63 (3), 387–405.

Chebbi, A., Carlier, P., 1996. Carboxylic acids in the troposphere, occurrence, sources, and sinks: a review. Atmos. Environ. 30 (24), 4233–4249.

Chen, M., Titcombe, M., Jiang, J., Jen, C., Kuang, C., Fischer, M.L., Eisele, F.L., Siepmann, J.I., Hanson, D.R., Zhao, J., 2012. Acid–base chemical reaction model for nucleation rates in the polluted atmospheric boundary layer. Proc. Natl. Acad. Sci. U.S.A. 109 (46), 18713–18718.

Chen, J., Jiang, S., Liu, Y.-R., Huang, T., Wang, C.-Y., Miao, S.-K., Wang, Z.-Q., Zhang, Y., Huang, W., 2017. Interaction of oxalic acid with dimethylamine and its atmospheric implications. RSC Adv. 7 (11), 6374–6388.

Chen, X., Zhao, Y.-F., Wang, L.-S., Li, J., 2017. Recent progresses of global minimum searches of nanoclusters with a constrained Basin-Hopping algorithm in the TGMin program. Comput. Theor. Chem. 1107, 57–65.

Contreras-García, J., Johnson, E.R., Keinan, S., Chaudret, R., Piquemal, J.-P., Beratan, D.N., Yang, W., 2011. NCIPLOT: a program for plotting noncovalent interaction regions. J. Comput. Chem. 7 (3), 625–632.

Frisch, M., Trucks, G., Schlegel, H., Scuseria, G., Robb, M., Cheeseman, J., Montgomery Jr., J., Vreven, T., Kudin, K., Burant, J., 2004. Gaussian 03, Revision C. 02, *26*.9. Gaussian, Inc., Wallingford, CT.

Galloway, J.N., Likens, G.E., Keene, W.C., Miller, J.M., 1982. The composition of precipitation in remote areas of the world. J. Geophys. Res.: Atmos: Oceans 87 (C11), 8771–8786.

Galvez, O., Gomez, P., Pacios, L., 2003. Variation with the intermolecular distance of properties dependent on the electron density in cyclic dimers with two hydrogen bonds. J. Chem. Phys. 118 (11), 4878–4895.

Gao, W., Jiao, J., Feng, H., Xuan, X., Chen, L., 2013. Natures of benzene-water and pyrrole-water interactions in the forms of σ and π types: theoretical studies from clusters to liquid mixture. J. Mol. Model. 19 (3), 1273–1283.

Ge, X., Wexler, A.S., Clegg, S.L., 2011. Atmospheric amines–Part II. Thermodynamic properties and gas/particle partitioning. Atmos. Environ. 45 (3), 561–577.

Granby, K., Christensen, C.S., Lohse, C., 1997. Urban and semi-rural observations of carboxylic acids and carbonyls. Atmos. Environ. 31 (10), 1403–1415.

Han, Y.-J., Feng, Y.-J., Miao, S.-K., Jiang, S., Liu, Y.-R., Wang, C.-Y., Chen, J., Wang, Z.-Q., Huang, T., Li, J., 2018. Hydration of 3-hydroxy-4, 4-dimethylglutaric acid with dimethylamine complex and its atmospheric implications. Phys. Chem. Chem. Phys. 20 (40), 25780–25791.

Herb, J., Nadykto, A.B., Yu, F., 2011. Large ternary hydrogen-bonded pre-nucleation clusters in the Earth's atmosphere. Chem. Phys. Lett. 518, 7–14.

Herb, J., Xu, Y., Yu, F., Nadykto, A., 2012. Large hydrogen-bonded pre-nucleation $(HSO_4^-)(H_2SO_4)_m$ $(H_2O)_k$ and $(HSO_4^-)(NH_3)(H_2SO_4)_m$ $(H_2O)_k$ clusters in the earth's atmosphere. J. Phys. Chem. A 117 (1), 133–152.

Hostaš, J., Řezáč, J., Hobza, P., 2013. On the performance of the semiempirical quantum mechanical PM6 and PM7 methods for noncovalent interactions. Chem. Phys. Lett. 568, 161–166.

Huang, X.-F., Hu, M., He, L.-Y., Tang, X.-Y., 2005. Chemical characterization of water-soluble organic acids in PM2. 5 in Beijing, China. Atmos. Environ. Times 39 (16), 2819–2827.

Huang, W., Pal, R., Wang, L.-M., Zeng, X.C., Wang, L.-S., 2010. Isomer identification and resolution in small gold clusters. J. Chem. Phys. 132 (5), 054305.

Humphrey, W., Dalke, A., Schulten, K., 1996. VMD: visual molecular dynamics. J. Mol. Graph. 14 (1), 33–38.

Jen, C.N., McMurry, P.H., Hanson, D.R., 2014. Stabilization of sulfuric acid dimers by ammonia, methylamine, dimethylamine, and trimethylamine. J. Geophys. Res.: Atmos. 119 (12), 7502–7514.

Jiang, S., Huang, T., Liu, Y.-R., Xu, K.-M., Zhang, Y., Lv, Y.-Z., Huang, W., 2014. Theoretical study of temperature dependence and Rayleigh scattering properties of chloride hydration clusters. Phys. Chem. Chem. Phys. 16 (36), 19241–19249.

Jokinen, T., Sipilä, M., Junninen, H., Ehn, M., Lönn, G., Hakala, J., Petäjä, T., Mauldin Iii, R., Kulmala, M., Worsnop, D., 2012. Atmospheric sulphuric acid and neutral cluster measurements using CI-APi-TOF. Atmos. Chem. Phys. 12 (9), 4117–4125.

Junninen, H., Ehn, M., Petäjä, T., Luosujärvi, L., Kotiaho, T., Kostiainen, R., Rohner, U., Gonin, M., Fuhrer, K., Kulmala, M., 2010. A high-resolution mass spectrometer to measure atmospheric ion composition. Atmos. Meas. Tech. 3 (4), 1039–1053.

Kildgaard, J.V., Mikkelsen, K.V., Bilde, M., Elm, J., 2018. Hydration of atmospheric molecular clusters II: organic acid–water clusters. J. Phys. Chem. A 122 (43), 8549–8556.

Kim, J., Mhin, B.J., Lee, S.J., Kim, K.S., 1994. Entropy-driven structures of the water octamer. Chem. Phys. Lett. 219 (3–4), 243–246.

Kuang, C., Riipinen, I., Sihto, S.-L., Kulmala, M., McCormick, A., McMurry, P., 2010. An improved criterion for new particle formation in diverse atmospheric environments. Atmos. Chem. Phys. 10 (17), 8469–8480.

Kulmala, M., 2003. How partical nucleate and grow. Science 302, 1000–1001.

Kulmala, M., Kerminen, V.-M., 2008. On the formation and growth of atmospheric nanoparticles. Atmos. Res. 90 (2–4), 132–150.

Kulmala, M., Vehkamäki, H., Petäjä, T., Dal Maso, M., Lauri, A., Kerminen, V.-M., Birmili, W., McMurry, P., 2004. Formation and growth rates of ultrafine atmospheric particles: a review of observations. J. Aerosol Sci. 35 (2), 143–176.

Kupiainen-Määttä, O., Henschel, H., Kurtén, T., Loukonen, V., Olenius, T., Paasonen, P., Vehkamäki, H., 2014. Comment on 'Enhancement in the production of nucleating clusters due to dimethylamine and large uncertainties in the thermochemistry of amine-enhanced nucleation'by Nadykto et al. Chem. Phys. Lett. 609, 42–49. Chem. Phys. Lett. **2015,** 624, 107-110.

Kurten, T., Sundberg, M.R., Vehkamäki, H., Noppel, M., Blomqvist, J., Kulmala, M., 2006. Ab initio and density functional theory reinvestigation of gas-phase sulfuric acid monohydrate and ammonium hydrogen sulfate. J. Phys. Chem. A 110 (22), 7178–7188.

Kurtén, T., Loukonen, V., Vehkamäki, H., Kulmala, M., 2008. Amines are likely to enhance neutral and ion-induced sulfuric acid-water nucleation in the atmosphere more effectively than ammonia. Atmos. Chem. Phys. 8 (14), 4095–4103.

Kurtén, T., Elm, J., Prisle, N.L., Mikkelsen, K.V., Kampf, C.J., Waxman, E.M., Volkamer, R., 2014. Computational study of the effect of glyoxal–sulfate clustering on the Henry's law coefficient of glyoxal. J. Phys. Chem. A 119 (19), 4509–4514.

Lanz, V.A., Alfarra, M.R., Baltensperger, U., Buchmann, B., Hueglin, C., Szidat, S., Wehrli, M.N., Wacker, L., Weimer, S., Caseiro, A., 2007. Source attribution of submicron organic aerosols during wintertime inversions by advanced factor analysis of aerosol mass spectra. Environ. Sci. Technol. 42 (1), 214–220.

Li, G., Zhang, R., Fan, J., Tie, X., 2005. Impacts of black carbon aerosol on photolysis and ozone. J. Geophys. Res.: Atmos. 110 (D23).

Limbeck, A., Puxbaum, H., Otter, L., Scholes, M.C., 2001. Semivolatile behavior of dicarboxylic acids and other polar organic species at a rural background site (Nylsvley, RSA). Atmos. Environ. 35 (10), 1853–1862.

Liu, Y.-R., Wen, H., Huang, T., Lin, X.-X., Gai, Y.-B., Hu, C.-J., Zhang, W.-J., Huang, W., 2014. Structural exploration of water, nitrate/water, and oxalate/water clusters with basin-hopping method using a compressed sampling technique. J. Phys. Chem. A 118 (2), 508–516.

Löflund, M., Kasper-Giebl, A., Schuster, B., Giebl, H., Hitzenberger, R., Puxbaum, H., 2002. Formic, acetic, oxalic, malonic and succinic acid concentrations and their contribution to organic carbon in cloud water. Atmos. Environ. 36 (9), 1553–1558.

Loukonen, V., Kurtén1, T., Ortega1, I.K., Vehkamäki1, H., Pádua2, A.A.H., Sellegri3, K., Kulmala1, M., 2010. Enhancing effect of dimethylamine in sulfuric acid nucleation in the presence of water – a computational study. Atmos. Chem. Phys. 10, 4961–4974.

Lv, G., Nadykto, A.B., Sun, X., Zhang, C., Xu, Y., 2018. Towards understanding the role of amines in the SO_2 hydration and the contribution of the hydrated product to new particle formation in the Earth's atmosphere. Chemosphere 205, 275–285.

Ma, J., Xia, X., Ma, Y., Luo, Y., Zhong, Y., 2018. Stability of dissolved percarbonate and its implications for groundwater remediation. Chemosphere 205, 41–44.

Maia, J.D.C., Urquiza Carvalho, G.A., Mangueira Jr., C.P., Santana, S.R., Cabral, L.A.F., Rocha, G.B., 2012. GPU linear algebra libraries and GPGPU programming for accelerating MOPAC semiempirical quantum chemistry calculations. J. Chem. Theory Comput. 8 (9), 3072–3081.

Makkonen, R., Asmi, A., Kerminen, V.-M., Boy, M., Arneth, A., Hari, P., Kulmala, M., 2012. Air pollution control and decreasing new particle formation lead to strong climate warming. Atmos. Chem. Phys. 12 (3), 1515–1524.

Martinelango, P.K., Dasgupta, P.K., Al-Horr, R.S., 2007. Atmospheric production of oxalic acid/oxalate and nitric acid/nitrate in the Tampa Bay airshed: parallel pathways. Atmos. Environ. 41 (20), 4258–4269.

McGrath, M., Olenius, T., Ortega, I., Loukonen, V., Paasonen, P., Kurtén, T., Kulmala, M., Vehkamäki, H., 2012. Atmospheric Cluster Dynamics Code: a flexible method for solution of the birth-death equations. Atmos. Chem. Phys. 12 (5), 2345–2355.

Merikanto, J., Spracklen, D., Mann, G., Pickering, S., Carslaw, K., 2009. Impact of nucleation on global CCN. Atmos. Chem. Phys. 9 (21), 8601–8616.

Mhin, B.J., Lee, S.J., Kim, K.S., 1993. Water-cluster distribution with respect to pressure and temperature in the gas phase. Phys. Rev. A 48 (5), 3764.

Miao, S.-K., Jiang, S., Chen, J., Ma, Y., Zhu, Y.-P., Wen, Y., Zhang, M.-M., Huang, W., 2015. Hydration of a sulfuric acid–oxalic acid complex: acid dissociation and its atmospheric implication. RSC Adv. 5 (60), 48638–48646.

Nadykto, A.B., Yu, F., 2007. Strong hydrogen bonding between atmospheric nucleation precursors and common organics. Chem. Phys. Lett. 435 (1–3), 14–18.

Nadykto, A.B., Al Natsheh, A., Yu, F., Mikkelsen, K.V., Herb, J., 2008. Computational quantum chemistry: a new approach to atmospheric nucleation. Adv. Quant. Chem. 55, 449–478.

Nadykto, A.B., Yu, F., Herb, J., 2008. Effect of ammonia on the gas-phase hydration of the common atmospheric ion HSO_4. Int. J. Mol. Sci. 9 (11), 2184–2193.

Nadykto, A.B., Yu, F., Herb, J., 2009. Theoretical analysis of the gas-phase hydration of common atmospheric pre-nucleation $(HSO_4^-)(H_2O)_n$ and $(H_3O^+)(H_2SO_4)(H_2O)_n$ cluster ions. Chem. Phys. 360 (1–3), 67–73.

Nadykto, A.B., Herb, J., Yu, F., Xu, Y., 2014. Enhancement in the production of nucleating clusters due to dimethylamine and large uncertainties in the thermochemistry of amine-enhanced nucleation. Chem. Phys. Lett. 609, 42–49.

Nadykto, A.B., Herb, J., Yu, F., Nazarenko, K.M., 2018. Clustering of highly oxidized organic acid with atmospheric NO_3^- and HSO_4^- ions and neutral species: thermochemistry and implications to new particle formation. Chem. Phys. Lett. 706, 175–181.

Noppel, M., Vehkamäki, H., Kulmala, M., 2002. An improved model for hydrate formation in sulfuric acid–water nucleation. J. Chem. Phys. 116, 218–228.

Olenius, T., Kupiainen-Määttä, O., Ortega, I., Kurtén, T., Vehkamäki, H., 2013. Free energy barrier in the growth of sulfuric acid–ammonia and sulfuric acid–dimethylamine clusters. J. Chem. Phys. 139 (8), 084312.

Ortega, I.K., Kurtén, T., Vehkamäki, H., Kulmala, M., 2008. The role of ammonia in sulfuric acid ion induced nucleation. Atmos. Chem. Phys. 8 (11), 2859–2867.

Ortega, I., Kupiainen, O., Kurtén, T., Olenius, T., Wilkman, O., McGrath, M., Loukonen, V., Vehkamäki, H., 2012. From quantum chemical formation free energies to evaporation rates. Atmos. Chem. Phys. 12 (1), 225–235.

Paasonen, P., Nieminen, T., Asmi, E., Manninen, H., Petäjä, T., Plass-Dülmer, C., Flentje, H., Birmili, W., Wiedensohler, A., Horrak, U., 2010. On the roles of sulphuric acid and low-volatility organic vapours in the initial steps of atmospheric new particle formation. Atmos. Chem. Phys. 10 (22), 11223–11242.

Peng, X.-Q., Liu, Y.-R., Huang, T., Jiang, S., Huang, W., 2015. Interaction of gas phase oxalic acid with ammonia and its atmospheric implications. Phys. Chem. Chem. Phys. 17 (14), 9552–9563.

Rozas, I., Alkorta, I., Elguero, J., 2000. Behavior of ylides containing N, O, and C atoms as hydrogen bond acceptors. J. Am. Chem. Soc. 122 (45), 11154–11161.
Ryding, M.J., Ruusuvuori, K., Andersson, P.U., Zatula, A.S., McGrath, M.J., Kurtén, T., Ortega, I.K., Vehkamäki, H., Uggerud, E., 2012. Structural rearrangements and magic numbers in reactions between pyridine-containing water clusters and ammonia. J. Phys. Chem. A 116 (20), 4902–4908.
Saikia, J., Narzary, B., Roy, S., Bordoloi, M., Saikia, P., Saikia, B.K., 2016. Nanominerals, fullerene aggregates, and hazardous elements in coal and coal combustion-generated aerosols: an environmental and toxicological assessment. Chemosphere 164, 84–91.
Saxon, A., Diaz-Sanchez, D., 2005. Air pollution and allergy: you are what you breathe. Nat. Immunol. 6 (3), 223.
Sipilä, M., Berndt, T., Petäjä, T., Brus, D., Vanhanen, J., Stratmann, F., Patokoski, J., Mauldin, R.L., Hyvärinen, A.-P., Lihavainen, H., 2010. The role of sulfuric acid in atmospheric nucleation. Science 327 (5970), 1243–1246.
Smith, J.N., Barsanti, K.C., Friedli, H.R., Ehn, M., Kulmala, M., Collins, D.R., Scheckman, J.H., Williams, B.J., McMurry, P.H., 2010. Observations of aminium salts in atmospheric nanoparticles and possible climatic implications. Proc. Natl. Acad. Sci. U.S.A. 107 (15), 6634–6639.
Temelso, B., Morrell, T.E., Shields, R.M., Allodi, M.A., Wood, E.K., Kirschner, K.N., Castonguay, T.C., Archer, K.A., Shield, G.C., 2012. Quantum mechanical study of sulfuric acid hydration: atmospheric implications. J. Phys. Chem. A 116, 2209–2224.
Vehkamäki, H., Kulmala, M., Napari, I., Lehtinen, K.E., Timmreck, C., Noppel, M., Laaksonen, A., 2002. An improved parameterization for sulfuric acid–water nucleation rates for tropospheric and stratospheric conditions. J. Geophys. Res.: Atmos. 107 (D22). AAC 3-1-AAC 3-10.
Wales, D.J., Doye, J.P., 1997. Global optimization by basin-hopping and the lowest energy structures of Lennard-Jones clusters containing up to 110 atoms. J. Phys. Chem. A 101 (28), 5111–5116.
Wang, C.-Y., Jiang, S., Liu, Y.-R., Wen, H., Wang, Z.-Q., Han, Y.-J., Huang, T., Huang, W., 2018. Synergistic effect of ammonia and methylamine on nucleation in the earth's atmosphere. A theoretical study. J. Phys. Chem. A 122 (13), 3470-347.
Weber, K.H., Morales, F.J., Tao, F.-M., 2012. Theoretical study on the structure and stabilities of molecular clusters of oxalic acid with water. J. Phys. Chem. A 116 (47), 11601–11617.
Wen, H., Huang, T., Wang, C.-Y., Peng, X.-Q., Jiang, S., Liu, Y.-R., Huang, W., 2018. A study on the microscopic mechanism of methanesulfonic acid-promoted binary nucleation of sulfuric acid and water. Atmos. Environ. 191, 214–226.
Wen, H., Wang, C.-Y., Wang, Z.-Q., Hou, X.-F., Han, Y.-J., Liu, Y.-R., Jiang, S., Huang, T., Huang, W., 2019. Formation of atmospheric molecular clusters consisting of methanesulfonic acid and sulfuric acid: insights from flow tube experiments and cluster dynamics simulations. Atmos. Environ. 199, 380–390.
Xu, W., Zhang, R., 2012. Theoretical investigation of interaction of dicarboxylic acids with common aerosol nucleation precursors. J. Phys. Chem. A 116 (18), 4539–4550.
Xu, W., Zhang, R., 2013. A theoretical study of hydrated molecular clusters of amines and dicarboxylic acids. J. Chem. Phys. 139 (6), 064312.
Xu, Y., Nadykto, A.B., Yu, F., Herb, J., Wang, W., 2009. Interaction between common organic acids and trace nucleation species in the earth's atmosphere. J. Phys. Chem. A 114 (1), 387–396.
Xu, Y., Nadykto, A.B., Yu, F., Jiang, L., Wang, W., 2010. Formation and properties of hydrogen-bonded complexes of common organic oxalic acid with atmospheric nucleation precursors. J. Mol. Struct. 951 (1–3), 28–33.
Zhang, R., Suh, I., Zhao, J., Zhang, D., Fortner, E.C., Tie, X., Molina, L.T., Molina, M.J., 2004. Atmospheric new particle formation enhanced by organic acids. Science 304 (5676), 1487–1490. *186, 78-87*.
Zhang, R., Li, G., Fan, J., Wu, D.L., Molina, M.J., 2007. Intensification of Pacific storm track linked to Asian pollution. Proc. Natl. Acad. Sci. U.S.A. 104 (13), 5295–5299.
Zhang, R., Wang, L., Khalizov, A.F., Zhao, J., Zheng, J., McGraw, R.L., Molina, L.T., 2009. Formation of nanoparticles of blue haze enhanced by anthropogenic pollution. Proc. Natl. Acad. Sci. U.S.A. 106 (42), 17650–17654.
Zhang, R., Khalizov, A., Wang, L., Hu, M., Xu, W., 2011. Nucleation and growth of nanoparticles in the atmosphere. Chem. Rev. 112 (3), 1957–2011.
Zhao, J., Levitt, N.P., Zhang, R., Chen, J., 2006. Heterogeneous reactions of methylglyoxal in acidic media: implications for secondary organic aerosol formation. Environ. Sci. Technol. 40 (24), 7682–7687.
Zhao, J., Khalizov, A., Zhang, R., McGraw, R., 2009. Hydrogen-bonding interaction in molecular complexes and clusters of aerosol nucleation precursors. J. Phys. Chem. A 113 (4), 680–689.
Zhao, J., Eisele, F.L., Titcombe, M., Kuang, C., McMurry, P.H., 2010. Chemical ionization mass spectrometric measurements of atmospheric neutral clusters using the cluster-CIMS. J. Geophys. Res.: Atmos. 115 (D8).
Zhao, J., Smith, J., Eisele, F., Chen, M., Kuang, C., McMurry, P., 2011. Observation of neutral sulfuric acid-amine containing clusters in laboratory and ambient measurements. Atmos. Chem. Phys. 11 (21), 10823–10836.
Zhao, Y., Chen, X., Li, J., 2017. TGMin: a global-minimum structure search program based on a constrained basin-hopping algorithm. Nano. Res. 10 (10), 3407–3420.
Zhu, Y.-P., Liu, Y.-R., Huang, T., Jiang, S., Xu, K.-M., Wen, H., Zhang, W.-J., Huang, W., 2014. Theoretical study of the hydration of atmospheric nucleation precursors with acetic acid. J. Phys. Chem. A 118 (36), 7959–7974.
Zobrist, B., Marcolli, C., Koop, T., Luo, B., Murphy, D., Lohmann, U., Zardini, A., Krieger, U., Corti, T., Cziczo, D., 2006. Oxalic acid as a heterogeneous ice nucleus in the upper troposphere and its indirect aerosol effect. Atmos. Chem. Phys. 6 (10), 3115–3129.